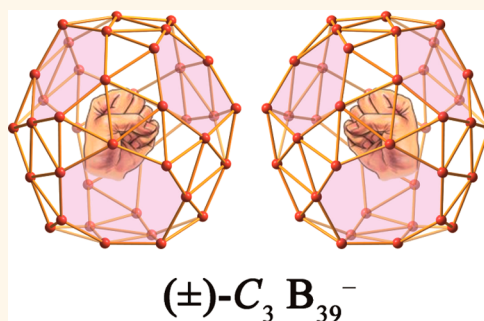# Experimental and Theoretical Evidence of an Axially Chiral Borospherene

Qiang Chen,[†] Wei-Li Li,[‡] Ya-Fan Zhao,[§] Su-Yan Zhang,[†] Han-Shi Hu,[§] Hui Bai,[†] Hai-Ru Li,[†] Wen-Juan Tian,[†] Hai-Gang Lu,[†] Hua-Jin Zhai,*,[†,⊥] Si-Dian Li,*,[†] Jun Li,*,[§] and Lai-Sheng Wang*,[‡]

[†]Nanocluster Laboratory, Institute of Molecular Science, Shanxi University, Taiyuan 030006, China, [‡]Department of Chemistry, Brown University, Providence, Rhode Island 02912, United States, [§]Department of Chemistry & Key Laboratory of Organic Optoelectronics and Molecular Engineering of Ministry of Education, Tsinghua University, Beijing 100084, China, and [⊥]State Key Laboratory of Quantum Optics and Quantum Optics Devices, Shanxi University, Taiyuan 030006, China

ABSTRACT Chirality plays an important role in chemistry, biology, and materials science. The recent discovery of the $B_{40}^{-/0}$ borospherenes marks the onset of a class of boron-based nanostructures. Here we report the observation of axially chiral borospherene in the B_{39}^{-} nanocluster on the bases of photoelectron spectroscopy, global minimum searches, and electronic structure calculations. Extensive structural searches in combination with density functional and CCSD(T) calculations show that B_{39}^{-} has a C_3 cage global minimum with a close-lying C_2 cage isomer. Both the C_3 and C_2 B_{39}^{-} cages are chiral with degenerate enantiomers. The C_3 global minimum consists of three hexagons and three heptagons around the vertical C_3 axis. The C_2 isomer is built on two

$(\pm)\text{-}C_3\ B_{39}^{-}$

hexagons on the top and at the bottom of the cage with four heptagons around the waist. Both the C_3 and C_2 axially chiral isomers of B_{39}^{-} are present in the experiment and contribute to the observed photoelectron spectrum. The chiral borospherenes also exhibit three-dimensional aromaticity, featuring σ and π double delocalization for all valence electrons. Molecular dynamics simulations reveal that these chiral B_{39}^{-} cages are structurally fluxional above room temperature, compared to the highly robust D_{2d} B_{40} borospherene. The current findings add chiral members to the borospherene family and indicate the structural diversity of boron-based nanomaterials.

Shortly after the discovery of the bulk synthesis of fullerenes,[1] the first axially chiral fullerene (D_2 C_{76}) was characterized experimentally.[2] As the lighter neighbor of carbon in the periodic table, boron is electron-deficient and its chemical bonding is dominated by multicenter bonds, resulting in the formation of polyhedral molecules and unusual crystal allotropes.[3,4] Since the first proposal of a possible B_{80} cage, built from a C_{60}-like B_{60} by filling each of the 20 hexagons with a B atom,[5] the pursuit of boron cages has attracted significant computational activity in the past several years.[6−14] However, subsequent calculations found that the putative B_{80} cage is not the global minimum, and the most favorable B_{80} structure is likely a core–shell type three-dimensional structure.[12,14−17] On the other hand, size-selected boron nanoclusters (B_n^{-} and B_n) have been shown in the past decade by systematic experimental and theoretical studies to be planar

or quasi-planar over a wide size range (n = 3−25, 30, 35, 36),[18−29] including the quasi-planar chiral B_{30}^{-} observed recently.[26] This leaves a relatively small size regime (∼37−70 atoms) for the possibility of all-boron cages. Very recently, we reported the first experimental and theoretical evidence for the existence of an all-boron fullerene at B_{40}.[30] Both B_{40} and its anion were found to have similar cage structures with D_{2d} symmetry. A name, borospherene, was suggested for the all-boron fullerene. The B_{40} borospherene is a slightly elongated cage, composed of interwoven double chains with two hexagons, one at the top and one at the bottom of the cage, and four heptagons on the waist.

In this contribution, we report a joint photoelectron spectroscopic and theoretical investigation on the B_{39}^{-} cluster, which is found to have an axially chiral C_3 global minimum with a low-lying C_2 axially chiral isomer. The B_{39}^{-} cluster represents the first borospherene with axial chirality as its

global minimum, suggesting that a new class of chiral borospherene-based nanostructures may exist. Chirality is important in chemistry, materials science, and biology. The observation of the axially chiral boron cage indicates the structural diversity of borospherenes, suggesting that much remains to be explored in low-dimensional boron nanomaterials.

RESULTS

Photoelectron Spectrum. The B_{39}^- cluster was produced *via* laser vaporization of a ^{10}B-enriched boron target and characterized using photoelectron spectroscopy (PES) (Figure 1a).[31] The leading PES band (X) has a vertical detachment energy (VDE) of 4.00(5) eV. Its well-defined onset allows the determination of an adiabatic detachment energy (ADE) of 3.84(5) eV, which represents the electron affinity (EA) of neutral B_{39}. The relatively large EA suggests that the B_{39}^- anion has a closed-shell electronic structure, and neutral B_{39} is
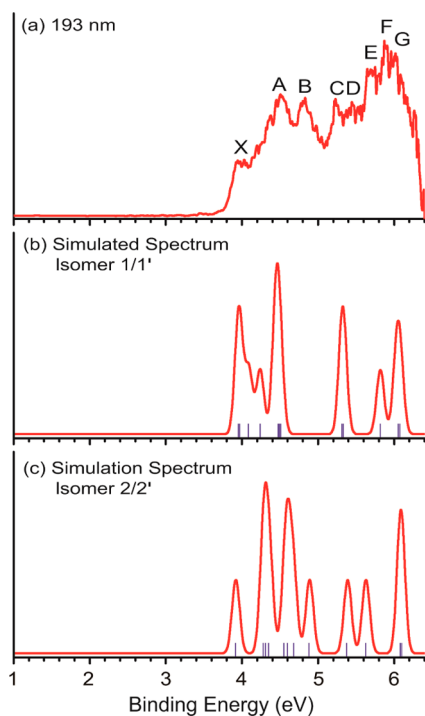
thus a superhalogen species. The next PES band (A) is observed at a VDE of 4.52 eV. Continuous electron signals exist in between bands X and A, suggesting additional, unresolved electronic transitions or possible contributions from coexisting isomers. Beyond band A, several well-defined bands are observed: B (4.82 eV), C (5.23 eV), D (5.45 eV), E (5.70 eV), F (5.88 eV), and G (6.00 eV). Overall, the PES pattern is rather congested and complicated, hinting that multiple isomers may be present in the B_{39}^- cluster beam.

Structural Searches. Global minimum searches for B_{39}^- were carried out using the Minima Hopping (MH) algorithm[32,33] at the density functional theory (DFT) level. Independent global minimum searches were also performed using the Basin Hopping (BH) method.[27] Low-lying structures were then fully optimized and their relative energies evaluated at both the DFT-PBE0[34] and CAM-B3LYP[35] levels with the 6-311+G* basis set.[36] Isomers within 1.5 eV at the PBE0 level are summarized in Figure S1 for B_{39}^- and Figure S2 for B_{39} in the Supporting Information. To obtain more accurate relative energies, single-point CCSD(T) calculations[37−39] with the optimized PBE0 geometries and the 6-311G* basis set were performed for the 12 lowest-lying isomers of B_{39}^-.

Figure 2 shows the global minimum C_3 structure of B_{39}^- at CCSD(T) level and the second lowest-lying C_2 isomer, which is only 0.08 eV above the C_3 isomer. The configurational energy spectrum of B_{39}^- is illustrated in Figure 3 at the single-point CCSD(T)//PBE0/6-311G* level. Interestingly, both C_3 and C_2 isomers are cages and are axially chiral. The degenerate global minima C_3(**1**) and C_3(**1'**) form a pair of axially chiral enantiomers with respect to the C_3 symmetry axis; the C_2(**2**) and C_2(**2'**) isomers also form a pair of axially chiral enantiomers about the C_2 symmetry axis. Among the first 12 most stable isomers at the CCSD(T) level, there are five additional cage isomers: C_1(**3**), C_1(**5**), C_1(**6**), C_2(**8**), and C_1(**10**), which are also chiral in nature (Figures 3 and S1). The first noncage isomer has a slightly distorted tubular structure (**4**, C_s).[20,40] The first quasi-planar isomer (**7**, C_s) is 0.28 eV above the global minimum at CCSD(T) and it is related to the recently observed hexagonal B_{36}^- cluster by attaching three B atoms along one edge.[27] Another quasi-planar isomer (**9**, C_s) has a central heptagonal hole.

Figure 1. Photoelectron spectrum of B_{39}^- at 193 nm (a), compared with the simulated spectra at PBE0 based on the C_3 B_{39}^- global minimum (b) and the low-lying C_2 B_{39}^- isomer (c). The vertical bars in (b) and (c) show the calculated VDEs.
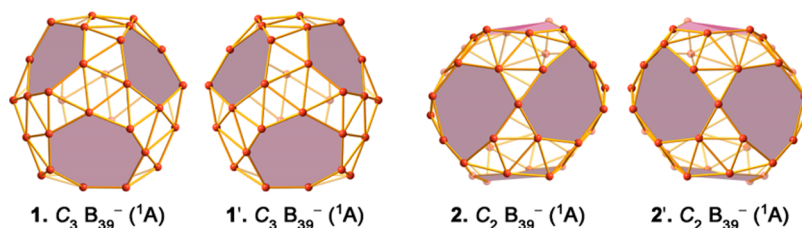

Figure 2. Optimized structures of the global minimum C_3 and close-lying C_2 isomers of B_{39}^-. The two enantiomers of the axially chiral structures are shown in each case. The hexagons and heptagons on the cage surface are shaded.
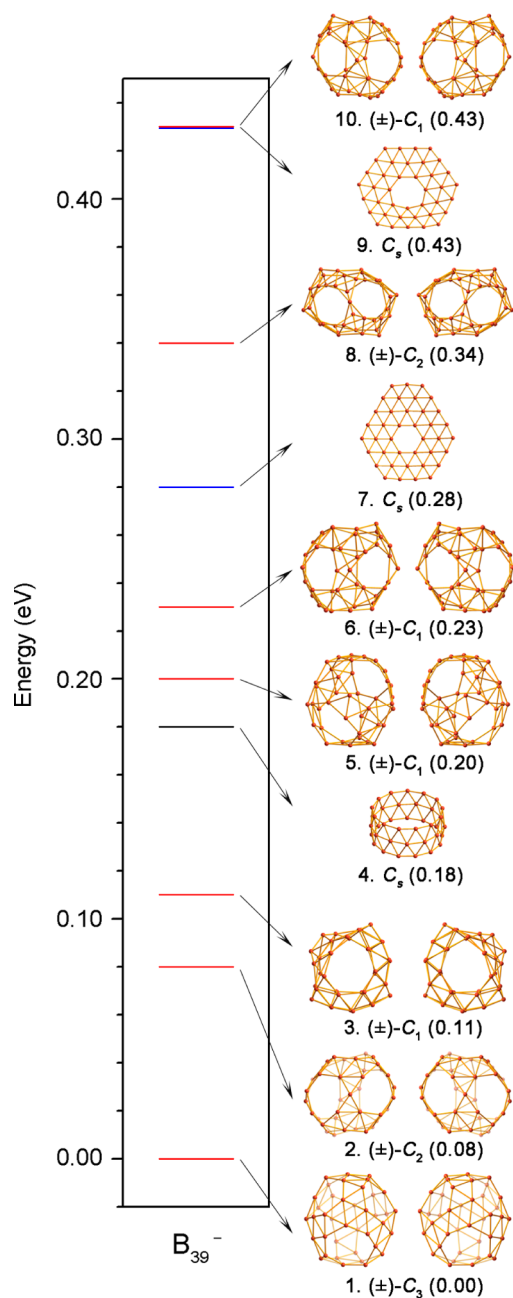
Figure 3. Configurational energy spectrum of B_{39}^- at the single-point CCSD(T)//PBE0/6-311G* level. The energy of the global minimum is taken to be zero, and the relative energies are in eV. Cage-like enantiomer pairs are degenerate in energy. The red, black, and blue bars denote fullerene-like cages, triple-ring tubes, and quasi-planar structures, respectively.

The potential energy surface of B_{39}^- is highly complicated with numerous close-lying local minima (Figures 3 and S1). At the PBE0 level, cage isomers **1**, **2**, and **3** are within 0.2 eV, whereas the tubular isomer **4** and planar isomer **7** are slightly lower in energy than **1** by 0.19 and 0.24 eV, respectively. However, at the CAM-B3LYP level, which includes the long-range correction using the Coulomb attenuating method,[35] the cage isomer **1** becomes the global minimum, but only 0.01 eV below isomer **7**. The CAM-B3LYP results are

reinforced by the more accurate CCSD(T) data. At our highest level of CCSD(T)//PBE0/6-311G*, isomer **1** remains the lowest in energy, closely followed by **2** at 0.08 eV higher. Isomers **3**−**6** are within 0.23 eV, whereas **7** is 0.28 eV higher in energy (Figure 3). On the basis of the energetics at CCSD(T), isomers **1**, **2**, and to a less extent, isomer **3**, may coexist experimentally and contribute to the observed PES spectrum. Note that B_{39}^- is the first case in boron anion clusters with a cage global minimum; the recently observed D_{2d} B_{40}^- borospherene is slightly higher than the planar global minimum, even though the neutral B_{40} borospherene is overwhelmingly the global minimum.[30] For neutral B_{39}, we only did PBE0 calculations (Figure S2). We found that the competition among cage, tubular, and quasi-planar structures remains, except that the triple-ring tubular isomer seems to be slightly more favored than in the anion case. The computational data also indicates that PBE0 biases toward quasi-planar or tubular structures, whereas CAM-B3LYP and the more reliable CCSD(T) favor cages.

Comparison between Experiment and Theory. To compare with the experimental data, we calculated the VDEs and simulated the PES spectra for the top 12 isomers, using the time-dependent DFT (TD-DFT) method.[41] Those from the two lowest energy isomers are compared with the experiment in Figure 1. The degenerate enantiomers of C_3(**1**) and C_2(**2**) should each produce the same PES spectra. The observed PES features X, A, C, F, and G are well reproduced by the simulated spectrum of the global minimum C_3(**1**) isomer (Figure 1b). The unresolved signals between bands X and A seem also to correspond to transitions of the C_3 isomer. However, the simulated spectrum of the C_3 isomer cannot explain all the observed PES bands, in particular, band B and the spectral region of D and E, which appear to come from the C_2(**2**) isomer (Figure 1c). Clearly, neither of the isomers alone can explain the observed spectrum. The combination of the two yields reasonable agreement with the experiment, providing credence for the coexistence of both the C_3 and C_2 isomers.

The simulated PES spectra for other low-lying cage isomers, **3**, **5**, **6**, **8**, and **10**, the tubular isomer **4**, and quasi-planar isomers **7**, **9**, **11**, and **13** are given in Figure S3. Because all these isomers are closed shell, they all give relatively high VDEs spanning the energy range of the experimental spectrum, except the isomer C_2(**8**), which has relatively low VDEs and can be ruled out. The situation of B_{39}^- is very different from B_{36}^- and B_{40}^-, where the neutral clusters are closed shell with large HOMO−LUMO gaps. The large energy gaps of B_{36} and B_{40} give rise to unusually low EAs for the neutral clusters. These spectral characteristics become defining features to unequivocally confirm the identified structures for the planar hexagonal $B_{36}^{-/0}$ cluster and the $B_{40}^{-/0}$ cage. For the complicated and congested spectrum of B_{39}^-, it is difficult to rule out safely any of the higher energy isomers based on the
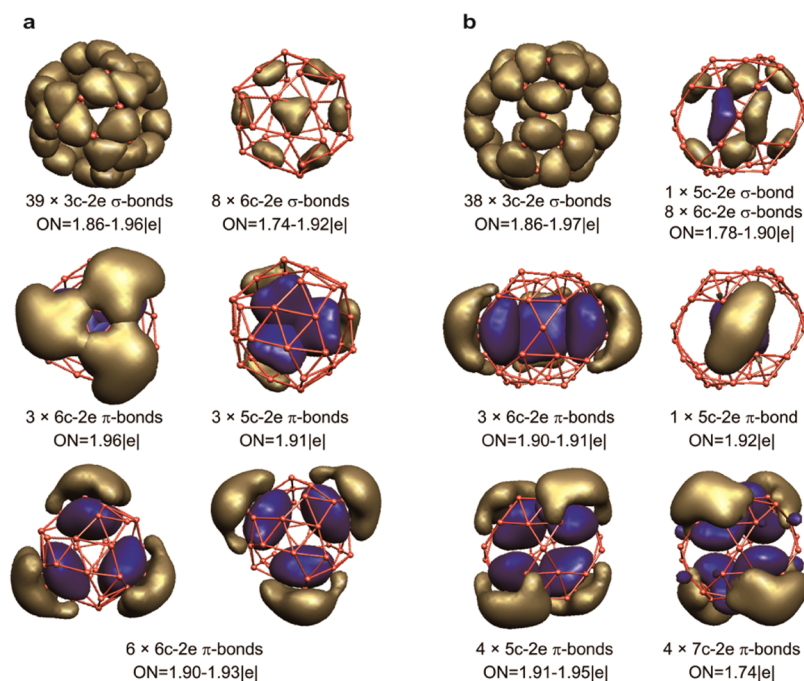
Figure 4. AdNDP bonding pattern for (a) the global minimum C_3 B_{39}^- and (b) the close-lying isomer C_2 B_{39}^-. The occupation numbers (ONs) are indicated.

comparison of the simulated and experimental data alone. However, previous investigations on a wide range of planar and cage-like boron clusters[18–30] show that the CCSD(T) level of theory gives reliable energetics information and should give sufficient credence for the identified C_3(**1**) and C_2(**2**) cage structures for B_{39}^-.

It is interesting to note that isomer **3** is the closest cage-like isomer with respect to C_3(**1**) and C_2(**2**). It also predicts the correct first VDE. However, its predicted transition at ~5.1 eV is in between the well-separated experimental bands B and C, suggesting that the population of **3** should be small, if any, in the cluster beam of B_{39}^-. The contributions from other low-lying isomers beyond isomer **3** should be negligible in terms of the energetics at the CCSD(T) level (Figure 3). Thus, despite the congestion of the observed PES spectrum of B_{39}^- (Figure 1a) and its complicated potential energy surface (Figure 3), the current combined experimental and computational data suggests that the chiral C_3 and C_2 isomers should be the correct assignment.

DISCUSSION

Axially Chiral Borospherene. The structure and bonding of the chiral C_3(**1**) and C_2(**2**) B_{39}^- can be compared with those of the B_{40} borospherene. Structurally, the C_3(**1**) B_{39}^- can be constructed from the B_{40} cage by replacing a B_7 heptagon with a B_6 hexagon, followed by a structural rearrangement. In fact, the C_3(**1**) B_{39}^- was obtained automatically during the MH searches, starting from an initial structure constructed from B_{40} by replacing a heptagon on its waist with a hexagon. Moreover, the C_2(**2**) B_{39}^- can be obtained from B_{40} by removal of one B

atom on the waist, so that one of the boron double chain on the waist is incomplete with a "defect" site.

The C_3(**1**) B_{39}^- cage contains three hexagons on the top, three heptagons at the bottom, and 47 triangles along the interwoven double chains around the vertical C_3 chiral axis, following Euler's rule: E (90 edges) $= F$ (47 triangular + 3 hexagonal + 3 heptagonal faces) + V (39 vertices) − 2. Electronically, the C_3(**1**) B_{39}^- is closed-shell with a large HOMO−LUMO gap of 2.89 eV at PBE0 (Figure S4), which is close to the corresponding value of 3.13 eV obtained for the B_{40} borospherene at the same level.[30]

Similarly, the C_2(**2**) B_{39}^- cage possesses a hexagon on the top and one at the bottom and four heptagons on the waist, consisting of 46 boron triangles also with a sizable HOMO−LUMO gap of 2.73 eV (Figure S4). The C_2(**2**) cage also conforms to Euler's rule: E (89 edges) $= F$ (46 triangular + 2 hexagonal + 4 heptagonal faces) + V (39 vertices) − 2.

Chemical Bonding: σ Plus π Double Delocalization. The chemical bonding of the C_3 and C_2 B_{39}^- cages is analyzed using the adaptive natural density partitioning (AdNDP) method (Figure 4).[42] The C_3 cage possesses 39 3c−2e and 8 6c−2e σ bonds (Figure 4a). For the 6c−2e σ bonds, the central B_3 triangles make major contributions. Thus, all 47 σ bonds are practically 3c−2e σ bonds, covering the cage surface uniformly with one σ bond for each B_3 triangle. The remaining 12 bonds form the delocalized π framework. The three 6c−2e and three 5c−2e π bonds are associated with the top and bottom B_6 triangles perpendicular to the C_3 symmetry axis, respectively. The six 6c−2e π bonds on the waist cover

the zigzag double chain between the top and bottom B_6 triangles. Thus, all the 118 valence electrons in the C_3 isomer are evenly delocalized over the cage surface in both the σ and π frameworks, which effectively compensates for boron's intrinsic electron deficiency. This bonding pattern is similar to that in the D_{2d} B_{40},[30] and it appears to be critical for the high stability of borospherenes.

Because of the less symmetric C_2 cage, an unusual 5c−2e σ bond is found (Figure 4b). It can be approximately viewed as a B 2p lone-pair. Indeed, the B atom at the "defect" site carries a negative natural charge of −0.60 $|e|$, unlike other B atoms in the cluster that are practically neutral. Other than that, the bonding pattern in the C_2 B_{39}^- is similar to that in the C_3 isomer. The 12 delocalized π bonds found in D_{2d} B_{40} are characteristic of borospherenes, and they are well maintained in both the C_3 and C_2 cages of B_{39}^-.

The bonding pattern of σ plus π double delocalization renders 3D aromaticity to the B_{39}^- borospherenes. Nucleus independent chemical shift (NICS)[43] calculations show that both the C_3 and C_2 B_{39}^- isomers have highly negative NICS values, −38 and −39 ppm, respectively, at the cage centers, which are comparable to the corresponding value of −42 ppm calculated for the B_{40} cage at the same theoretical level.[30]

The C_3/C_2 B_{39}^- borospherenes can be further stabilized by binding with an alkali counterion to form a neutral, charge-transfer complex, $M^+B_{39}^-$. Figure S4 shows the cases of two C_1 $Li^+B_{39}^-$ species, in which Li^+ caps a heptagon face. The cage-like $Li^+B_{39}^-$ complexes are also chiral with HOMO−LUMO gaps comparable to those of the parent B_{39}^- cluster and neutral D_{2d} B_{40}.

Cube-Like Cages and Analogy to Cubane (C_8H_8). The chemical bonding of the B_{40} and B_{39}^- borospherenes can be further understood by comparing with that of the cubane (C_8H_8), similar to the analogy between the bonding of planar boron clusters and that of polycyclic aromatic hydrocarbons.[18,19,22−29] The D_{2d} B_{40} and the two chiral isomers, C_3 and C_2, of B_{39}^- can be viewed to possess cube-like cage structures with the six hexagonal or heptagonal holes as the faces and the eight B_6 triangles as the corners of the cube (Figure S5). As deduced from the AdNDP analyses, each B_6 triangle effectively contributes 3 electrons to the π framework, facilitating the global bonding of the B_6 triangle to its three neighboring B_6 units. The 12 delocalized π bonds over the σ skeleton in borospherenes resemble the 12 C−C bonds in cubane.

Molecular Dynamics of B_{39}^-: A "Glassy" Form of Nanoboron? To further explore the stability of the B_{39}^- chiral borospherenes, we carried out molecular dynamics (MD) simulations at the DFT level.[44] At 200 K, the C_3 isomer is dynamically stable during the 30 ps MD simulations (Figure S6). At 300 K and especially at 500 K, however, the B_{39}^- cluster starts to "hop" between different cage structures *via* concerted mechanisms with low energy barriers. The transformations involve synergetic bond breakage and formation, mainly between the C_3 and C_2 isomers, with small contributions from other low-lying cage-like isomers. Note that in the MD simulations, the $C_2(\mathbf{2})$ isomer seems to be dynamically more stable than the global minimum $C_3(\mathbf{1})$ isomer. This observation suggests that the relative population of C_3 versus C_2 isomers may vary, depending on experimental conditions.

The dynamical behavior of the cube-like B_{39}^- indicates that it is structurally fluxional above room temperature and may be viewed as a "glassy" form of nanoboron, much like a Rubik's cube with various permutations, hinting that the B_{39}^- cluster probably has a significantly lower melting point than bulk boron (2349 K). It should be pointed out that this behavior is size-dependent, because certain boron cages are more robust than others. For example, the B_{40} borosphere is dynamically stable even at 1000 K.[30] As already mentioned above, the C_3 and C_2 borospherenes, and other cage-like structures in Figure 3 as well, are composed of interwoven boron double chain nanoribbons. Such nanoribbons also make two-dimensional boron sheet or even a nanotube.[45] The current results show again the robustness of boron double chain nanoribbons in low-dimensional boron nanostructures. The chiral C_3 and C_2 B_{39}^- borospherenes may serve as valuable models for mechanistic understanding of the nucleation and growth of chiral boron nanotubes. Indeed, the "defect" site in C_2 B_{39}^- and the unique dynamic behaviors of C_3 and C_2 B_{39}^- should better facilitate the growth of chiral boron nanotubes.

CONCLUSIONS

In conclusion, we have observed the first axially chiral B_{39}^- borospherene, which are found to have two close-lying, chiral isomers with C_3 and C_2 symmetries. Both isomers are shown to be present experimentally and contribute to the observed photoelectron spectrum of B_{39}^-. These axially chiral borospherenes possess 3D aromaticity and are characterized with σ plus π double delocalization in chemical bonding, similar to the B_{40} borosphere. The chiral cages are shown to be dynamically fluxional above room temperature. The current findings introduce chiral members to the borospherene family and indicate the structural diversity of the borospherene-based nanostructures.

METHODS SECTION

Photoelectron Spectroscopy. The experiment was done using a magnetic-bottle-type photoelectron spectroscopy apparatus,[31] equipped with a laser vaporization supersonic cluster source.

Briefly, the B_{39}^- clusters were produced using a [10]B-enriched boron disk target in the presence of a helium carrier gas seeded with 5% argon and were mass selected using a time-of-flight mass spectrometer. The B_{39}^- cluster was selected and photodetached

by a 193 nm photon beam from an ArF excimer laser. Photoelectron spectrum was obtained using a 3.5 m long electron flight tube and was calibrated using the known spectrum of Au^-. The energy resolution of the magnetic-bottle electron analyzer was $\Delta E/E \approx 2.5\%$, that is, ~25 meV for 1 eV kinetic energy electrons.

Computational Methods. The MH algorithm[32,33] and TGmin program[27] were employed independently to search for the global minimum of B_{39}^-. MH is based on the principle of exploring the configurational space as fast as possible and of avoiding revisiting known parts of this space, which proves to be an efficient global minimum search algorithm for the potential energy surface of complex molecular systems. The MH calculations were carried out using the BIGDFT electronic structure code,[46] which is based on a systematic wavelet basis in combination with pseudopotentials and the standard local-density approximation (LDA)[47] and Perdew−Burke−Ernzerhof (PBE)[48] exchange-correlation functionals. Initial structures are primarily based on those of the recently studied B_{40} cluster[30] by removing one B atom, further aided by manual structural constructions. About 5000 isomers were found from 8 independent MH searches, which include the low-lying C_3 and C_2 cage-like structures and their enantiomers.

To confirm the results of the MH searches, TGmin searches were also conducted. This involves the improved BH algorithm, which was carried out using the DFT formalism with the PBE exchange-correlation functional and the Goedecker−Teter−Hutter (GTH) pseudopotential[47] with the associated double-z valence plus polarization (DZVP) basis set[49] using the CP2K program.[44] TGmin is a highly parallelized global optimization program. Starting from a given initial seed structure, it automatically generates displaced structures and input files for geometry optimization. Multiple geometry optimization jobs are submitted to the batch system on the computing platform. To identify duplicated structures, structural similarity comparison is carried not only after the geometry optimization, but also during the geometry optimization. This kind of on-the-fly comparison notably reduced the CPU time for geometry optimization, thus increasing the efficiency of the global minimum search. More than 4600 isomers were produced via TGmin and no isomer is more stable than the C_3 structure and its enantiomer.

All low-lying isomers obtained from MH and TGmin searches were reoptimized at the PBE0/6-311+G*[34,36] and CAM-B3LYP/6-311+G*[35,36] levels using the Gaussian 09 program[50] and each reported isomer was ensured to be true minimum through frequency calculations. For more accurate relative energies, the optimized structures at PBE0 level were further evaluated via single-point CCSD(T)//PBE0/6-31G*[37−39,51] and CCSD(T)//PBE0/6-311G* calculations using the Molpro package.[52] For the neutral B_{39} clusters, structures corresponding to the low-lying isomers of B_{39}^- within 1 eV relative to the C_3 structure at PBE0/6-311+G* were calculated using the same method. The VDEs of low-lying anion isomers were calculated using the TD-DFT method.[41] Chemical bonding analyses were performed using AdNDP[42] and visualized using Molekel.[53] Molecular dynamics simulations were performed using the software suite CP2K.[44]

Conflict of Interest: The authors declare no competing financial interest.

Supporting Information Available: Alternative optimized structures for B_{39}^- and B_{39}, simulated photoelectron spectra of alternative low-lying isomers, comparison of the HOMO−LUMO gaps of B_{39}^- and $Li^+B_{39}^-$ with that of B_{40}, comparison of the structures of B_{39}^- and B_{40} with cubane C_8H_8, molecular dynamics simulations, and the coordinates of the two lowest-lying chiral structures. This material is available free of charge via the Internet at http://pubs.acs.org.

REFERENCES AND NOTES

1. Krätschmer, W.; Lamb, L. D.; Fostiropoulos, K. D.; Huffman, D. R. Solid C_{60}: A New Form of Carbon. *Nature* **1990**, *347*, 354–358.
2. Ettl, R.; Chao, I.; Diederich, F.; Whetten, R. L. Isolation of C_{76}, a Chiral (D_2) Allotrope of Carbon. *Nature* **1991**, *353*, 149–153.
3. Lipscomb, W. N. The Boranes and Their Relatives. *Science* **1977**, *196*, 1047–1055.
4. Albert, B.; Hillebrecht, H. Boron: Elementary Challenge for Experimenters and Theoreticians. *Angew. Chem., Int. Ed.* **2009**, *48*, 8640–8668.
5. Szwacki, N. G.; Sadrzadeh, A.; Yakobson, B. I. B_{80} Fullerene: An *Ab Initio* Prediction of Geometry, Stability, and Electronic Structure. *Phys. Rev. Lett.* **2007**, *98*, 166804. Erratum: *Phys. Rev. Lett.* **2008**, *100*, 159901.
6. Sheng, X. L.; Yan, Q. B.; Zheng, Q. R.; Su, G. Boron Fullerenes B_{32+8k} with Four-Membered Rings and B_{32} Solid Phases: Geometrical Structures and Electronic Properties. *Phys. Chem. Chem. Phys.* **2009**, *11*, 9696–9702.
7. Wang, L.; Zhao, J. J.; Li, F. Y.; Chen, Z. F. Boron Fullerenes with 32−56 Atoms: Irregular Cage Configurations and Electronic Properties. *Chem. Phys. Lett.* **2010**, *501*, 16–19.
8. Zhao, J. J.; Wang, L.; Li, F. Y.; Chen, Z. F. B_{80} and Other Medium-Sized Boron Clusters: Core-Shell Structures, Not Hollow Cages. *J. Phys. Chem. A* **2010**, *114*, 9969–9972.
9. Zope, R. R.; Baruah, T. Snub Boron Nanostructures: Chiral Fullerenes, Nanotubes and Planar Sheet. *Chem. Phys. Lett.* **2011**, *501*, 193–196.
10. Özdoğan, C.; Mukhopadhyay, S.; Hayami, W.; Guvenc, Z. B.; Pandy, R.; Boustani, I. The Unusually Stable B_{100} Fullerene, Structural Transitions in Boron Nanostructures, and a Comparative Study of α-and γ-Boron and Sheets. *J. Phys. Chem. C* **2010**, *114*, 4362–4375.
11. Quarles, K. D.; Kah, C. B.; Gunasinghe, R. N.; Musin, R. N.; Wang, X. Q. Filled Pentagons and Electron Counting Rule for Boron Fullerenes. *J. Chem. Theory Comput.* **2011**, *7*, 2017–2020.
12. De, S.; Willand, A.; Amsler, M.; Pochet, P.; Genovese, L.; Goedecker, S. Energy Landscape of Fullerene Materials: A Comparison of Boron to Boron Nitride and Carbon. *Phys. Rev. Lett.* **2011**, *106*, 225502.
13. Polad, S.; Ozay, M. A New Hole Density as a Stability Measure for Boron Fullerenes. *Phys. Chem. Chem. Phys.* **2013**, *15*, 19819–19824.
14. Lv, J.; Wang, Y. C.; Zhu, L.; Ma, Y. M. B_{38}: An All-Boron Fullerene Analogue. *Nanoscale* **2014**, *6*, 11692–11696.
15. Prasad, D. L. V. K.; Jemmis, E. D. Stuffing Improves the Stability of Fullerenelike Boron Clusters. *Phys. Rev. Lett.* **2008**, *100*, 165504.
16. Shang, B.; Yuan, L. F.; Zeng, X. C.; Yang, J. L. *Ab Initio* Prediction of Amorphous B_{84}. *J. Phys. Chem. A* **2010**, *114*, 2245–2249.
17. Li, F. Y.; Jin, P.; Jiang, D. E.; Wang, L.; Zhang, S. B.; Zhao, J. J.; Chen, Z. F. B_{80} and $B_{101−103}$ Clusters: Remarkable Stability of the Core-Shell Structures Established by Validated Density Functionals. *J. Chem. Phys.* **2012**, *136*, 074302.
18. Zhai, H. J.; Alexandrova, A. N.; Birch, K. A.; Boldyrev, A. I.; Wang, L. S. Hepta- and Octacoordinate Boron in Molecular Wheels of Eight- and Nine-Atom Boron Clusters: Observation and Confirmation. *Angew. Chem., Int. Ed.* **2003**, *42*, 6004–6008.
19. Zhai, H. J.; Kiran, B.; Li, J.; Wang, L. S. Hydrocarbon Analogues of Boron Clusters—Planarity, Aromaticity and Antiaromaticity. *Nat. Mater.* **2003**, *2*, 827–833.
20. Kiran, B.; Bulusu, S.; Zhai, H. J.; Yoo, S.; Zeng, X. C.; Wang, L. S. Planar-to-Tubular Structural Transition in Boron Clusters: B_{20} as the Embryo of Single-Walled Boron Nanotubes. *Proc. Natl. Acad. Sci. U. S. A.* **2005**, *102*, 961–964.
21. Oger, E.; Crawford, N. R. M.; Kelting, R.; Weis, P.; Kappes, M. M.; Ahlrichs, R. Boron Cluster Cations: Transition from Planar to Cylindrical Structures. *Angew. Chem., Int. Ed.* **2007**, *46*, 8503–8506.
22. Sergeeva, A. P.; Zubarev, D. Yu.; Zhai, H. J.; Boldyrev, A. I.; Wang, L. S. A Photoelectron Spectroscopic and Theoretical

Study of B_{16}^- and B_{16}^{2-}: An All-Boron Naphthalene. *J. Am. Chem. Soc.* **2008**, *130*, 7244–7246.

23. Huang, W.; Sergeeva, A. P.; Zhai, H. J.; Averkiev, B. B.; Wang, L. S.; Boldyrev, A. I. A Concentric Planar Doubly π-Aromatic B_{19}^- Cluster. *Nat. Chem.* **2010**, *2*, 202–206.

24. Sergeeva, A. P.; Piazza, Z. A.; Romanescu, C.; Li, W. L.; Boldyrev, A. I.; Wang, L. S. B_{22}^- and B_{23}^-: All-Boron Analogues of Anthracene and Phenanthrene. *J. Am. Chem. Soc.* **2012**, *34*, 18065–18073.

25. Popov, I. A.; Piazza, Z. A.; Li, W. L.; Wang, L. S.; Boldyrev, A. I. A Combined Photoelectron Spectroscopy and *Ab Initio* Study of the Quasi-Planar B_{24}^- Cluster. *J. Chem. Phys.* **2013**, *139*, 144307.

26. Li, W. L.; Zhao, Y. F.; Hu, H. S.; Li, J.; Wang, L. S. $[B_{30}]^-$: A Quasiplanar Chiral Boron Cluster. *Angew. Chem., Int. Ed.* **2014**, *53*, 5540–5545.

27. Piazza, Z. A.; Hu, H. S.; Li, W. L.; Zhao, Y. F.; Li, J.; Wang, L. S. Planar Hexagonal B_{36} as a Potential Basis for Extended Single-Atom Layer Boron Sheets. *Nat. Commun.* **2014**, *5*, 3113.

28. Sergeeva, A. P.; Popov, I. A.; Piazza, Z. A.; Li, W. L.; Romanescu, C.; Wang, L. S.; Boldyrev, A. I. Understanding Boron Through Size-Selected Clusters: Structure, Chemical Bonding, and Fluxionality. *Acc. Chem. Res.* **2014**, *47*, 1349–1358.

29. Li, W. L.; Chen, Q.; Tian, W. J.; Bai, H.; Zhao, Y. F.; Hu, H. S.; Li, J.; Zhai, H. J.; Li, S. D.; Wang, L. S. The B_{35} Cluster with a Double-Hexagonal Vacancy: A New and More Flexible Structural Motif for Borophene. *J. Am. Chem. Soc.* **2014**, *136*, 12257–12260.

30. Zhai, H. J.; Zhao, Y. F.; Li, W. L.; Chen, Q.; Bai, H.; Hu, H. S.; Piazza, Z. A.; Tian, W. J.; Lu, H. G.; Wu, Y. B.; Mu, Y. W.; Wei, G. F.; Liu, Z. P.; Li, J.; Li, S. D.; Wang, L. S. Observation of an All-Boron Fullerene. *Nat. Chem.* **2014**, *6*, 727–731.

31. Wang, L. S.; Cheng, H. S.; Fan, J. Photoelectron Spectroscopy of Size-Selected Transition Metal Clusters: Fe_n^-, $n = 3-24$. *J. Chem. Phys.* **1995**, *102*, 9480–9493.

32. Goedecker, S. Minima Hopping: An Efficient Search Method for the Global Minimum of the Potential Energy Surface of Complex Molecular Systems. *J. Chem. Phys.* **2004**, *120*, 9911–9917.

33. Goedecker, S.; Hellmann, W.; Lenosky, T. Global Minimum Determination of the Born-Oppenheimer Surface within Density Functional Theory. *Phys. Rev. Lett.* **2005**, *95*, 055501.

34. Adamo, C.; Barone, V. Toward Reliable Density Functional Methods without Adjustable Parameters: The PBE0 Model. *J. Chem. Phys.* **1999**, *110*, 6158–6170.

35. Yanai, T.; Tew, D.; Handy, N. C. A New Hybrid Exchange-Correlation Functional Using the Coulomb-Attenuating Method (CAM-B3LYP). *Chem. Phys. Lett.* **2004**, *393*, 51–57.

36. Krishnan, R.; Binkley, J. S.; Seeger, R.; Pople, J. A. Self-Consistent Molecular Orbital Methods. XX. A Basis Set for Correlated Wave Functions. *J. Chem. Phys.* **1980**, *72*, 650–654.

37. Čížek, J. On the Use of the Cluster Expansion and the Technique of Diagrams in Calculations of Correlation Effects in Atoms and Molecules. *Adv. Chem. Phys.* **1969**, *14*, 35–89.

38. Purvis, G. D., III; Bartlett, R. J. A Full Coupled-Cluster Singles and Doubles Model: The Inclusion of Disconnected Triples. *J. Chem. Phys.* **1982**, *76*, 1910–1918.

39. Raghavachari, K.; Trucks, G. W.; Pople, J. A.; Head-Gordon, M. A Fifth-Order Perturbation Comparison of Electron Correlation Theories. *Chem. Phys. Lett.* **1989**, *157*, 479–483.

40. Tian, F. Y.; Wang, Y. X. The Competition of Double-, Four-, and Three-Ring Tubular B_{3n} ($n = 8-32$) Nanoclusters. *J. Chem. Phys.* **2008**, *129*, 024903.

41. Bauernschmitt, R.; Ahlrichs, R. Treatment of Electronic Excitations within the Adiabatic Approximation of Time Dependent Density Functional Theory. *Chem. Phys. Lett.* **1996**, *256*, 454–464.

42. Zubarev, D. Yu.; Boldyrev, A. I. Developing Paradigms of Chemical Bonding: Adaptive Natural Density Partitioning. *Phys. Chem. Chem. Phys.* **2008**, *10*, 5207–5217.

43. Schleyer, P. v. R.; Maerker, C.; Dransfeld, A.; Jiao, H.; Hommes, N. J. v. E. Nucleus-Independent Chemical Shifts: A Simple and Efficient Aromaticity Probe. *J. Am. Chem. Soc.* **1996**, *118*, 6317–6318.

44. VandeVondele, J.; Krack, M.; Mohamed, F.; Parrinello, M.; Chassaing, T.; Hutter, J. QUICKSTEP: Fast and Accurate Density Functional Calculations Using a Mixed Gaussian and Plane Waves Approach. *Comput. Phys. Commun.* **2005**, *167*, 103–128.

45. Singh, A. K.; Sadrzadeh, A.; Yakobson, B. I. Probing Properties of Boron α-Tubes by *Ab Initio* Calculations. *Nano Lett.* **2008**, *8*, 1314–1317.

46. Genovese, L.; Neelov, A.; Goedecker, S.; Deutsch, T.; Ghasemi, S. A.; Willand, A.; Caliste, D.; Zilberberg, O.; Rayson, M.; Bergman, A.; Schneider, R. Daubechies Wavelets as a Basis Set for Density Functional Pseudopotential Calculations. *J. Chem. Phys.* **2008**, *129*, 014109.

47. Goedecker, S.; Teter, M.; Hutter, J. Separable Dual-Space Gaussian Pseudopotentials. *Phys. Rev. B: Condens. Matter Mater. Phys.* **1996**, *54*, 1703–1710.

48. Perdew, J. P.; Burke, K.; Ernzerhof, M. Generalized Gradient Approximation Made Simple. *Phys. Rev. Lett.* **1996**, *77*, 3865–3868.

49. VandeVondele, J.; Hutter, J. Gaussian Basis Sets for Accurate Calculations on Molecular Systems in Gas and Condensed Phases. *J. Chem. Phys.* **2007**, *127*, 114105.

50. Frisch, M. J.; Trucks, G. W.; Schlegel, H. B.; Scuseria, G. E.; Robb, M. A.; Cheeseman, J. R.; Scalmani, G.; Barone, V.; Mennucci, B.; Petersson, G. A.; *et al. Gaussian 09*, Revision B.01; Gaussian Inc., Wallingford, CT, 2010.

51. Dill, J. D.; Pople, J. A. Self-Consistent Molecular Orbital Methods. XV. Extended Gaussian-Type Basis Sets for Lithium, Beryllium, and Boron. *J. Chem. Phys.* **1975**, *62*, 2921–2922.

52. Werner, H. J.; Knowles, P. J.; Knizia, G.; Manby, F. R.; Schütz, M.; Celani, P.; Korona, T.; Lindh, R.; Mitrushenkov, A.; Rauhut, G.; *et al. MOLPRO*, version 2012.1.

53. Varetto, U. *Molekel 5.4.0.8*; Swiss National Supercomputing Center: Manno, Switzerland, 2009.